Analyzing the Effect of Olivine Mineralization on the Strength of the Oceanic Lithosphere

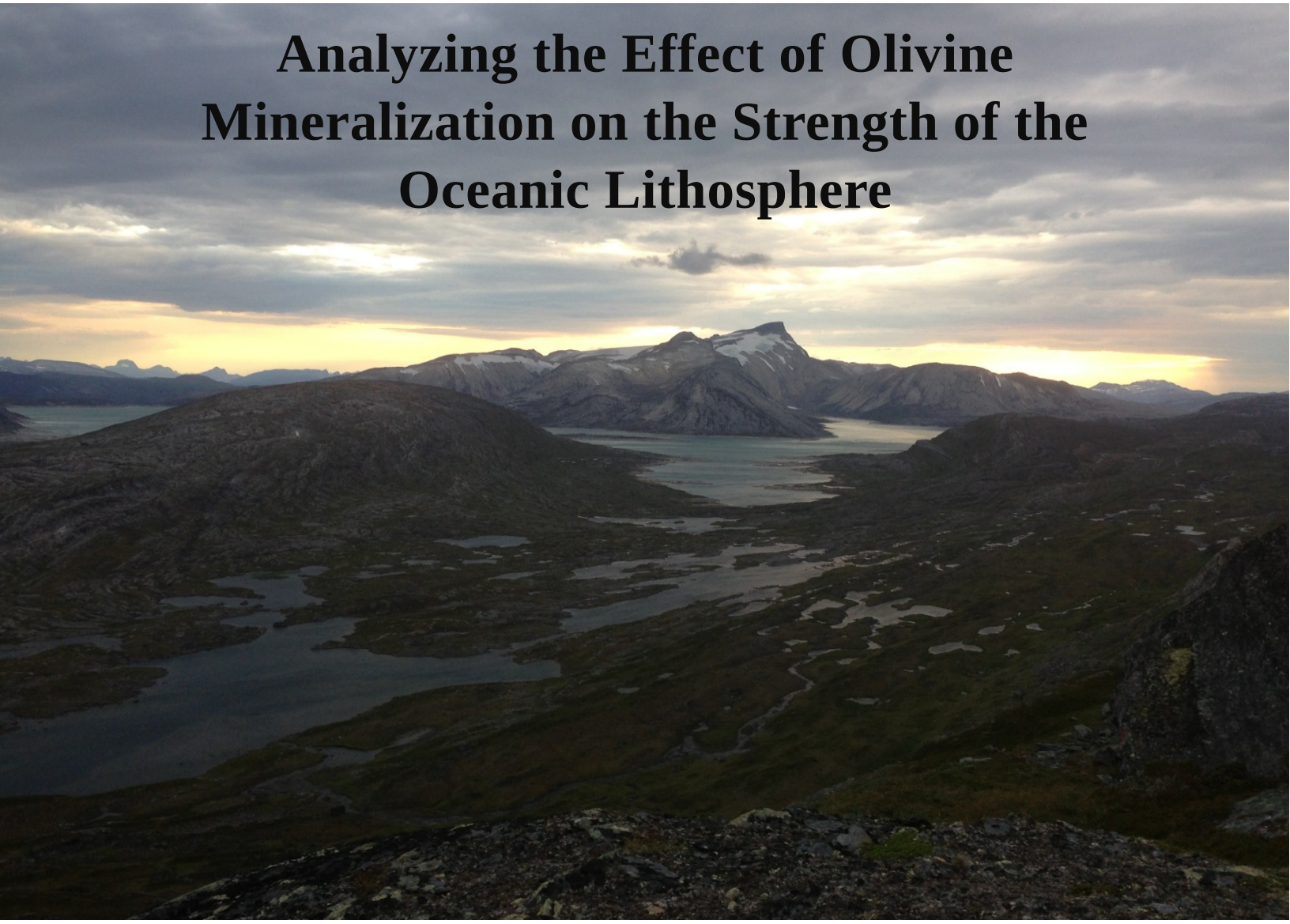

Thomas Braga

Advisor: Dr. Zhu

Co-advisor: H. Lisabeth

April 28th, 2014

Senior Thesis 394

Abstract:

The strength of the lithosphere has been defined by the maximum load it can withstand without breaking. Constraints of the strength of oceanic lithosphere come from deformational experiments of olivine. From experimental observations of samples from present and ancient seafloors, it is clear that olivine carbonation is an integrated part of the formation and evolution of the oceanic lithosphere. Studies show that olivine mineralization occurs when olivine reacts with H_2O and dissolved CO_2 to form hydrous silicates (e.g. serpentine), Fe-oxides (e.g. magnetite), and carbonates (e.g. calcite, magnesite, and dolomite). With increased mineralization, a transformation from olivine to serpentine to the final product being some combination of the minerals talc, magnesite, and quartz (listvenite). This induces a major change in the brittle shear strength of the rock. Currently, the change in shear strength due to olivine carbonation has not been quantified.

My experiments have been set-up to test various properties of samples collected from an outcrop in Norway, which hosts large quantities of obducted oceanic lithosphere. I have recorded properties such as porosity, elastic moduli, and shear strength. My hypothesis states that as peridotite in the oceanic lithosphere is mineralized, the shear strength of the rock is reduced. This can have implications on tectonic plate movement and fault activity. Also, this research can be contributed to studies which have been considering the idea of CO_2 sequestration using ultramafic rocks. As part of my design, I have tested samples of serpentinite, soapstone, and dunite. The intention of this study is to better constrain the strength of the oceanic lithosphere, by quantifying the shear strength of the main rocks present within.

I. Introduction

The theory of plate tectonics has great explanatory power and can account for mountain building, earthquakes, as well as many other deformational events. The plates constitute the lithosphere, which encompasses the Earth's uppermost mantle and the crust. The lithosphere bears loads over geological time. The strength of the lithosphere is the maximum load that it can withstand without breaking. The maximum strength of lithosphere cannot exceed the strength of the rocks that it is made of. The continental lithosphere consists primarily of granitic rock, whereas the oceanic lithosphere contains basaltic rocks (Burov, 2011). The strength of rocks can vary significantly with a sensitive to mineralogy, grain size, porosity, interstitial fluids, as well as pressure, temperature, and types of loads (Paterson and Wong, 2005).

Currently, constraints of the strength of oceanic lithosphere come from deformation experiments on olivine. At low temperatures, olivine rocks deform in a brittle regime, in which fracture occurs once the load exceed the rock strength. At temperatures of 600°C and above, experiments conducted on olivine demonstrated that its wet rheology is much weaker than the dry rheology (Kohlsted et al., 1995).

It has been stated that water circulates in the upper crust of the oceanic lithosphere (Adelinet et al., 2013). Olivine mineralization occurs when olivine reacts with H_2O and dissolved CO_2 to form hydrous silicates (e.g. serpentine), Fe-oxides (e.g. magnetite), and carbonates (e.g. calcite, magnesite, and dolomite). With progressed alteration, there is a transformation from

olivine to serpentine with the final product being some combination of the minerals talc, magnesite, and quartz (listvenite).

Observations of both present seafloor and ancient seafloor obducted on land show that olivine carbonation is an integrated part of the formation and evolution of the oceanic lithosphere. For example, it is estimated that 10-30% of basement rock found at crustal levels (depths < 7 km below seafloor) which occur at slow and ultra-slow spreading ridges, consist of serpentinized peridotite. Deformation experiments on slightly serpentinized peridotite samples demonstrate that small amounts of serpentine will significantly weaken peridotite (Escartin et al., 2001). Comparisons to unaltered dunite (Escartin et al., 2001) show that the shear strength of peridotite with ~10% lizardite and chrysotile serpentine is much lower, exhibiting a strength similar to pure serpentinite.

Carbonation of ultramafic rocks characterizes an important change as the process alters the properties of the protolith (Plumper et al., 2012). Norway hosts large outcrops of naturally carbonated peridotite rocks. The process olivine carbonation generates a major change in rock's brittle shear strength. However to date, the change in shear strength due to olivine carbonation is unknown. As part of my study, I have conducted brittle deformation experiments on dunite, serpentine, and soapstone. In practice, dunite is used as a proxy to unaltered peridotite due to its olivine content (~90%) as well as its presence within ophiolites. I have compared the brittle strength of these rocks to provide a better constraint for the overall strength of the oceanic lithosphere.

II. Hypotheses

a. The hydration of peridotite reduces the shear strength of the rock as it is altered to serpentinite.
b. The carbonation of serpentinite will further reduce the shear strength of the rock, as it becomes altered into soapstone.

Null Hypothesis

a. The hydration and carbonation of peridotite will have no affect at all on the strength of the rock.

I intend on testing this hypothesis, by running a series of experiments during which I will record properties including the samples elastic moduli and shear strengths. If I find that there is no significant difference in the overall strengths of the different rocks then my hypothesis will have been falsified and the null hypothesis will be accepted.

III. Sample Collection

A majority of the samples used for this study were collected from an outcrop in Linnajavri, Norway, which hosts large outcrops of ophiolites. Ophiolites have been produced from the obduction of lithospheric material from the sea floor. This area of Norway is said to have formed during the suprasubduction setting of the North Iapetus Ocean (Plumper et al., 2012). Ophiolites can preserve the metamorphic history of the oceanic lithosphere (Plumper et al., 2012) and this region hosts serpentinized ultra mafic rocks and carbonated peridotites such as

soapstone and listvenite. From analyzing rocks these rocks, we can better understand olivine mineralization and its effect on the oceanic lithosphere.

a. Locality

The ultramafic rocks studied in Linnajavri are centered near the region found at 67°36'N and 16°24'E. This encompasses the border of Sweden and includes the areas of Gaskavarri and Ridoalggicohkka (Beinlich et al. 2012). It is suggested that these rocks were accumulated from Caledonian nappes which were positioned above a Precambrian granite basement (Lindahl and Nilsson, 2008). The magnitude of geology in this area is dominated by tectonic nappes and thrust sheets, separated by thrust fault planes. In the northeastern region of Linnajavri there can be found Koli and Seve nappes. Nearby are dense and heavily altered zones of tectonic mélange. The tectonic mélanges consist of long, narrow zones of crushed and metasomatically altered rocks (Lindahl and Nilsson, 2008). These rocks have preferentially developed where serpentinite and soapstone rocks originated.

b. Mineralization of olivine

The upper crust of the oceanic lithosphere is consists of mafic basalts. It has been established that as basalt lavas cool they become extremely fractured. At shallow depths these cracks can host fluids which can initiate serpentinization (Adelinet et al., 2013), (Escartin et al., 1997). The oceanic mantle is mostly peridotite rock which consists of ultramafic rocks and ~ 60% olivine. Olivine is the most robust mineral found within the oceanic lithosphere. It is for this reason that studying the strength of olivine bearing rocks and its altered phases is important in understanding the overall strength of oceanic lithosphere.

Mineralization and alteration found in the oceanic lithosphere are strongly associated with volatile mediated mineral reactions. The most evident of these reactions are the hydration (serpentinization) of mantle peridotite and the dehydration of serpentinites. These two reactions have fundamental ramifications to the physical responses observed in the oceanic lithosphere (Plumper et al., 2012). The oceanic lithosphere can be hydrated at shallow depths where the temperatures are relatively low. It is observed that the hydration of olivine yields minerals such as serpentine and brucite, which are found in serpentinites.

$$2Mg_2SiO_4 + 3H_2O \rightarrow Mg_3Si_2O_5\,(OH)_4 + Mg\,(OH)_2$$

olivine + water → serpentine + brucite

Lizardite and chrysotile are the most common serpentine phases found in oceanic rocks. Geophysical data implies indicate that serpentinites are a major component of the oceanic lithosphere (Escartin et al., 2001). Although it has been stated that serpentinite is weaker than unaltered peridotite (Escartin et al, 2001), serpentinite is not a weak rock. Deformational experiments done with temperatures of ~25°C, show that core samples of serpentinite possess strength comparable to granite (Raleigh & Paterson, 1965).

c. Mineralization of serpentinite

The soapstone deposits found in Linnajavri formed as a result of the exposure of serpentinized ultramafic rocks to hot fluids, which were enriched in dissolved CO_2 (Lindahl and Nilsson, 2008). The serpentinites, which formed in many area of the outcrop from hydrated peridotites, responded with the formation of talc and magnesite. These two minerals found in abundance within the soapstones studied in this region (Lindahl and Nilsson, 2008).

$$2Mg_3Si_2O_5(OH)_4 + 3CO_2 \rightarrow Mg_3Si_4O_{10}(OH)_2 + 3MgCO_3 + 3H_2O$$

$$\text{serpentine} + CO_2 \rightarrow \text{talc} + \text{magnesite} + \text{water}$$

There are several zones of soapstone which display primary magmatic textures, inherited from dunite and peridotite. In Kleberflaget, a large deposit of soapstone in Linnajavri, there are segments of the ophiolite complexes identified as mantle material. (Lindahl and Nilsson, 2008). Many of the deformational structures are preserved in the soapstone. Structures such as joints, fissures, and minor textural features from the serpentinite protolith are noticeable in the soapstone (Lindahl and Nilsson, 2008).

d. Mineralization of soapstone

The abundance of CO_2 was so large that the soapstone continued to react with the CO_2, after the serpentinite was depleted. The result was the formation of listvenite deposits in Kleberflaget. Listvenite is a rock that consists primarily of quartz and magnesite and can be produced from talc carbonation.

$$Mg_3Si_4O_{10}(OH)_2 + 3CO_2 \rightarrow 4SiO_2 + 3MgCO_3 + H_2O$$

$$\text{talc} + CO_2 \rightarrow \text{quartz} + \text{magnesite} + \text{water}$$

According to Lindahl and Nilsson (2008) the formation of listvenite is the strongest indication and confirmation that the soapstone was not produced from a sedimentary source (e.g. calcite, dolomite marble, and black shale). They stated they were confident that the CO_2 was consequent of a robust and long-lasting mantle source from an early oceanic stage. This source is suggested to have been active over a range that included low temperatures (200-300°C). This would be below the lower stability of talc in ultramafic rocks, which proposes a reason for the transition of talc to quartz and additional magnesite which is found in the soapstone (Lindahl and Nilsson, 2008).

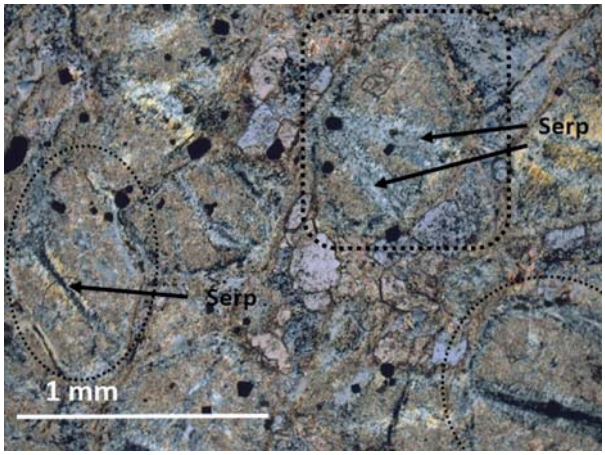

Figure 1: Serpentinite thin section (XPL, 5x magnification) Dashed lines point out pseudomorph structures. Arrows point at serpentine which has infiltrated cracks that were present in the olivine. Photo provided by Harrison

IV. Microstructural Analysis of Starting Materials

a. Serpentinite

From the analysis of the photomicrographs containing serpentinite, I have concluded that the amount of serpentinite

minerals falls within the range of 70-90%. The other minerals present are a combination opaque minerals and orthopyroxene. The grain sizes range between .25-1 mm. The serpentine was identified by the fibrous texture, low birefringence, and interference colors of 1st order grey and yellow (figure 1). Many of the preexistent olivine grains have been replaced by serpentine, which are observed as pseudomorph structures. Additionally, serpentine veins separate nearly all the olivine minerals (Plumper, Piazolo, & Austrheim, 2012). The pore spaces in the rocks have been thoroughly filled by the serpentine veins which can reduce porosity of the rock.

b. Soapstone

From the examination of the photomicrographs containing soapstone, I observed quantities of talc minerals between 25-35%. Correspondingly the thin section contained 45-55% serpentinite minerals. The remaining 10% of the minerals were opaque minerals (solid black) and some remaining orthopyroxene

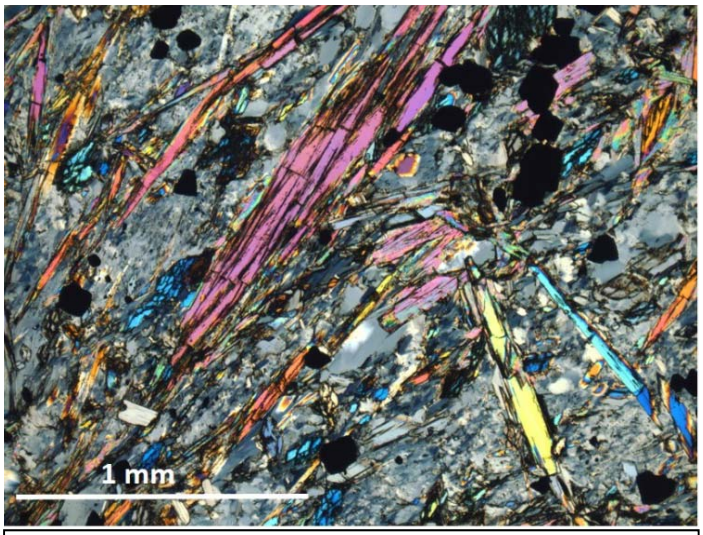

Figure 2: Soapstone thin section (XPL, 5x magnification) Talc grains identified by purple and green grains. Photograph provided by Harrison Lisabeth.

The grain sizes range between .25-1.4 mm. The talc has recognized by the micaceous texture, high birefringence, and interference colors of 3rd order purple and green. The image on the right (figure 2) displays talc grains with a random orientation. This can be associated with the growth of post-tectonic crystals which formed metamorphically, during dehydration of serpentine minerals.

Thin sections of the samples post-deformation are not yet available. This analysis may be available by the time of the poster presentation.

V. Physical Properties

I tested my hypotheses by examining the behavior of samples of dunite, serpentinite, and soapstone. The samples were cut into right cylinders. There were two sets of dimensions: length ~38.3 mm and diameter ~18.45 mm and length ~25.6 mm and diameter ~12.75 mm. With the equipment in the rock physics lab I observed and recorded the following rock properties of my samples: porosity, elastic wave speed, shear strength and electrical resistivity.

a. Porosity

Porosity is the quantity of void space within the rock in comparison to the total volume of the material. This property is observed to better understanding the transportation of ions in solution and how the materials are exposed to alteration. I measured the porosity of the samples using an Ultra Pore 300 He Porosimeter System. Due to complications, I was not able to use the apparatus to record the porosities of dunite. This most likely due to its low porosity and the range

of sensitivity of the machine (0.01 – 40.0%). Additionally there was some damage done to the soapstone samples through this process (figure 3).

Figure 3: Soapstone sample fractured with a low confining pressure of 300 kPa.

As an alternative, I recorded the porosity by recording the mass of a saturated sample and the mass of the sample dry and then calculated the difference in mass. This value is divided by the denisity of water used in the saturate the sample. This is equivalent to the volume of the connected void spaces. The volume of the connected void space is then divided by the total volume of the material, yielding the porosity of the samples.

Porosity: $$\phi = \frac{V_v}{V_T} \quad [1]$$

b. Stress

Stress (σ), in respect to load (i.e. weight), is considered a contact force. When the force of load exceeds the strength of the material, the stress will cause deformation to the body of material. This deformation is quantified as strain. Strain (ε) is a tensor, which measures the amount of deformation an object has undergone in comparison to its original dimensions. As part of my experimental set-up I have measured the radial strain (ε_r), the axial strain (ε_a), and I calculated the volumetric strain (ε_v). The axial and radial strain are measured by the Autolab 1500 apparatus. Volumetric strain can be totaled from the axial and radial strain recorded.

Volumetric Strain: $$\varepsilon_v = \varepsilon_a + 2\varepsilon_r \quad [2]$$

Rheology is the study of how rocks respond to stress (Davis et al. 2012). Experimentally, this is done by exposing rocks to forces and stresses under controlled conditions in the laboratory. From observations, we can mathematically describe the patterns of deformation and the relationship between stress and strain (Davis et al., 2012). The oceanic lithosphere is composed of many different types of rocks. So to better interpret the relationship between stress and strain, we need to study several rocks, rather than only one, to more accurately describe its behavior.

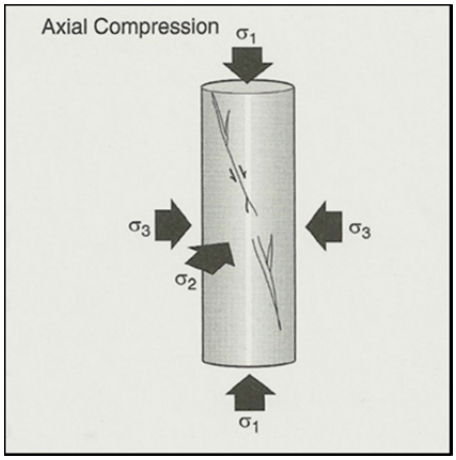

Figure 4: Image depicting compressive stress on the sample during axial compression (Davis et al.

During most of the experiments, the stresses imposed on the samples were hydrostatic. This means that the compressive stresses (figure 4) are equal in all directions, in all three directions ($\sigma_1 = \sigma_2 = \sigma_3$). While executing the deformation experiment, I wanted to study the in situ response of the oceanic lithosphere to loading. To accomplish this, there needs to be one primary stressor, while the other

two stressors are equal. The least compressive stresses are kept constant while the primary compressive stress is continually rising. The difference between the greatest and least compressive stress is differential stress.

Differential stress: $\sigma_1 - \sigma_3$ [3]

c. *Elastic Modulus*

As part of the deformation experiments, the samples are subjected to conditions with cumulative axial loading. A plot graph of differential stress vs axial strain from on such experiment should contain a segment of the graph which appears linear with a positive slope. At any point in this linear segment, if you were to remove the stress from the experiment, the sample would return to its original shape and size. This property is referred to as elasticity. Elasticity is the property that will returns an object such as a rubber band to its original shape when tensile stress is removed from the rubber band. There is a straight-line or liner relationship solids display during loading or unloading during elastic deformation (Davis et al. 2012).

During the experiments I have conducted, I have characterized the following elastic properties: the Young's modulus, Poisson's ratio, and shear modulus. The value calculated for the Young's modulus is recoreded from the slope of the linear portion of a differetial stress/axial strain curve. This curve tracks the progressive stress levels achieved during the loading of the rock samples (Davis et al., 2012) and the corresponding strain achieved.

Young's modulus: $E = \frac{\Delta\sigma}{\varepsilon_a}$ [4]

The Poisson's ratio (ν) is the negative ratio of transverse to axial strain. When a material is compressed in one direction, it will typically expand in the other two directions perpendicular to the direction of axial compression. This result is called the Poisson effect and the Poisson's ratio is a measure of this effect. The value for the Poisson's ratio is dimensionless and between zero and one ($0 < \nu < 1$).

Poisson's Ratio: $\nu = \frac{-\varepsilon_r}{\varepsilon_a}$ [5]

The shear modulus (G), describes the sample's response to shear stress in the experiments. The shear modulus can be calculated from the Young's modulus and the Poisson's ratio which were recorded during the deformation experiments. The velocities of shear waves (Vs) are controlled by the shear modulus. Shear waves are also referred to as secondary waves which are one of the two main types of elastic body waves, which move through the interior of the earth

Shear Modulus: $G = \frac{E}{2(1+\nu)}$ [6]

Shear Wave: $V_s = \sqrt{\frac{G}{\rho}}$ [7]

As part of my experiments I also recorded the elastic wave velocities of the samples (table 2). The velocity can be determined by the time elapsed in traveling the distance by the wave pulse from the emitter to the receiver end transducer in the rock sample (Khandelwal, 2013). The sample is placed within the experimental conditions, as the confining pressure increases the compressional wave (V_p) speeds are recorded. The wave velocity of the sample is dependent on the density and elastic properties of that material (Khandelwal, 2013). During loading, the applied stress to the samples can close grains, microcracks, and pore spaces (Asef & Najibi, 2013); as a result, the mechanical behavior of the sample will behave more elastically.

d. Shear Strength

Rock fracturing with low to moderate confining pressure results in the formation of dilatant cracks, followed by localization along shear zones (Kohlstedt et al., 1995). The model of the Mohr circle combined with the equation of Coulomb's failure criterion has been applied to represent this relationship (figure 5). This formula is calculated from the normal force, σ_n, which is multiplied by the angle of internal friction, ϕ. This value in addition to the cohesion of the material, C, quantifies the shear stress required to generate failure in the rock.

Coulomb's law of failure: $\tau = \sigma_n(\tan\phi) + C$ [8]

Past studies have estimated the upper limit for the strength of the lithosphere based on results collected during laboratory measurements of the mechanical properties of rocks (Kohlstedt et al., 1995). It has been suggested that the strength of Earth cannot be any larger than the strength of the rocks from which it is composed of (Kohlstedt et al., 1995). The peak load that a material can bear before failure is considered to represent the shear strength of the rock. This concept is applied in the design of my experiments and used to approximate the overall strength of the main rock found in the oceanic lithosphere.

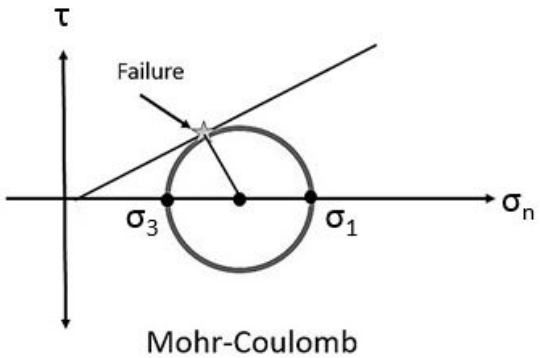

Figure 5: This image depicts a Mohr circle combined with the Coulomb failure criterion. As the stress applied to the sample reaches the envelope of failure (angled line in image based on angle of internal friction) the sample reached failure, denoted by the star.

It is noted that serpentinite has a comparable strength at standard room temperature; however, as temperature increases from ~25˚C to 200˚C, the strength of serpentine is reduced to less than half that value (Raleigh & Paterson, 1965). Lizardite serpentine, present in serpentinite, is stable up to ~350-400˚C (Escartin et al., 1997). Deformation observed in lizardite is primarily encompassed along the basal plane with the development of shear cracks. It is due to this property that lizardite has a low coefficient of internal friction ~0.3 (Escartin et al., 1997). These characteristics will have a considerable effect on the strength of rocks possessing this mineral.

Talc is stable up to temperatures of 800°C and pressures up to 5 GPa (Escartin et al., 2008). Frictional experiments conducted with talc show that the mineral has an extremely low angle of internal friction, $\phi = 0.14$ (Escartin et al., 2008). Similarly to other brittle rocks, strain weakening has been associated with localized deformation, which proceeds sliding along faults (Escartin et al., 2008). During the experiment with talc set to room temperature, the failure was associated with the formation will of a localized shear zone. It is suggested that the presence of talc could affect the entire thickness of the lithosphere and faults resulting it strength reduction and localized strain (Escartin et al., 2008).

e. Resistivity

Resistivity is explained through Ohm's law. The electric resistivity (R) of a material is measured in ohm meters (Ωm). The procedure of this experiment passes an electrical current (I) through a medium. The potential difference (V), measured in volts, is calculated from the time travel compared to the distance travelled by the current. Resistivity is used to study oxidation-reduction reactions as well as reactions due to ion exchanges (Olkoeft, 1985).

Ohm's Law: $V = IR$ [9]

VI. Experimental procedure

The experiments were conducted in the rock physics lab using the servo-controlled Autolab 1500 axial deformation apparatus (figure 6). The apparatus comprises of a pressure vessel with a hydraulic piston which applies the axial stress. There is also a pore pressure system with upstream and downstream servo-controlled intensifiers, which provides independent control over the pore pressure. The piston displacements are recorded by linear variable displacement transformers which carry a range of 76.2 mm, a sensitivity of 0.0254 mm, and an error less than 0.0015. The axial stress is measured by an internal load cell with a range of 0-1 GPa and an error less than 0.0044. The confining pressure and pore pressure transducers have a range of 0-137.9 MPa and the differential pressure transducer has a range of 0-206.84 MPa; all of which have an error less than 0.005 (Lisabeth et al., 2012).

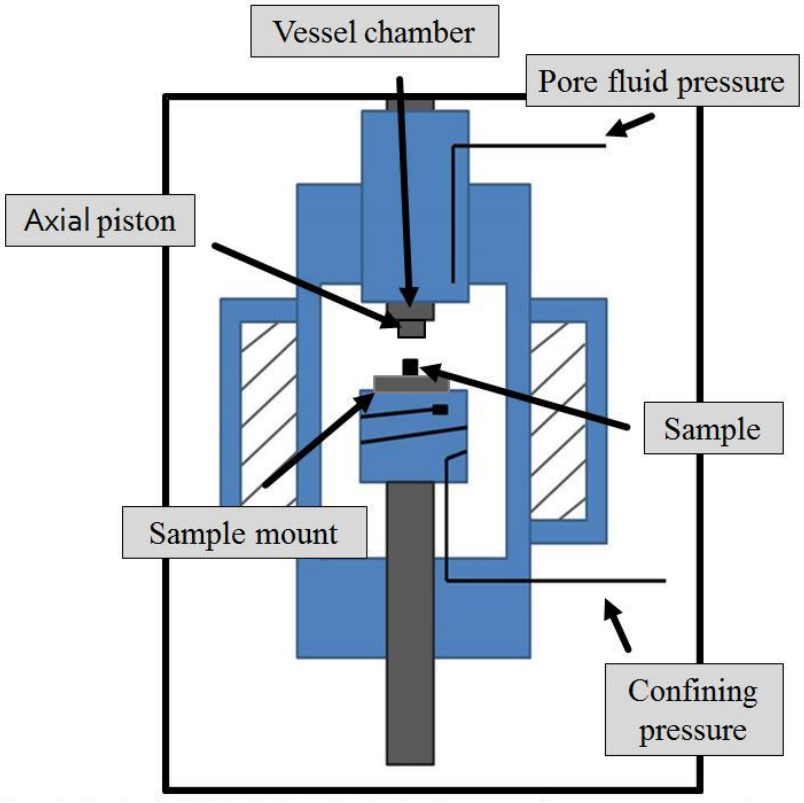

Figure 6: Schematic of Autolab 1500 axial deformation apparatus with significant areas of interest.

The samples were drilled from the outcrop using a gas powered Tanaka field drill the core samples. After the design of experiments was decided upon, the core samples were sent out to be cut into right cylinders of specific dimensions.

The technique used to collect the sample's electrical resistivity is as follows: we saturate the sample in a brine of known conductivity. The sample is then affixed to resistivity sample holders, wrapped in a non-conductive jacket, and clamped with metal wires. The sample and holder are then loaded into the pressure vessel. After the vessel is sealed the confining pressure is raised to 3 MPa and pore pressure is raised to 1 MPa. The pressure and temperature within the chamber is raised to the experimental conditions. A reference resistor is selected with comparable resistance to the sample. A voltage of several different frequencies is passed through the sample and the sample resistivity data is collected for analysis.

The method for collecting a sample's seismic velocity is as follows. The sample is cased in a heat sealed jacket and clamped to the velocity sample holders with wire. On one side of the sample is attached a piezo-electric transducer and on the other end a sensor to receive the seismic waves. The sample is then affixed to the sample holder with ultra-sonic velocity heads. The pressure vessel is sealed and raised to the experimental conditions. A broadband ultrasonic pulse is sent through the sample and the time travel is recorded. The seismic velocity for the sample is then calculated from the travel time of the elastic waves through the sample and the sample length.

Sample preparation for deformation experiment is done in this manner. First the sample is measured to record its precise length and diameter before strain is induced. Then a copper foil is marked with a digital ruler to the circumference of the sample with the excess of ~2-3 mm for the solder weld. The copper is then cut and wrapped around the specimen and bound with a rubber band on either end. Using the solder iron, there are welds placed on both ends and one in the middle. The rubber band is then removed and a smooth weld is placed along the edge of the copper foil. This is done carefully so there are no uneven lumps of iron, which would create a gap between the sample and sample holder for confining fluid to infiltrate. The copper foil is then sanded which adds a texture to the surface. Afterward, strain gauges are attached to the copper by strong epoxy glue. The sample is then placed in a heat shrinking casing with an extra length of ~7-10 mm on either end. The specimen is then placed on a vice with a

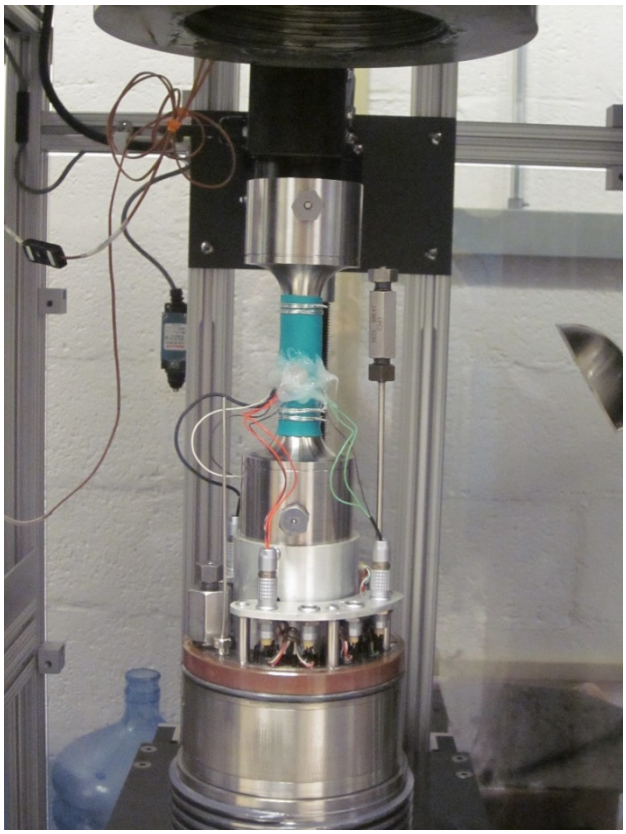

Figure 7: Sample has been prepared with strain gauges, proper jacketing, and loaded into the Autolab 1500 apparatus.

sample holder on either end. The vice is important because it will remove any gaps between the sample and the sample holder. A gap would provide the sample room to shift, while in the apparatus. The casing is then shrunk with a heat gun; you should see a crease on either end where the sample meets the sample holder. Wire is then wrapped on either end, past the sample on the excess area covering the sample holder. The wire is wrapped around thrice, tightened, and the excess is clipped close to the sample.

The strain gauges are attached to the copper foil with one positioned in the axial direction and one placed in the radial direction. The sample is then placed in a heat sealed jacket with wire tied to either end. Next the sample is affixed to the deformation sample holder (figure 7). The vessel is then sealed and filled with mineral oil, which will act as the confining pressure of the experiment. A confining pressure of 50 MPa is set for the experiment. Then the axial piston is lowered until it makes contact with the sample holder. This will introduce the axial stress component of the experiment. The piston is then advanced at a constant displacement rate which corresponds to a constant nominal strain rate. The stress and strain behavior is monitored by the computer system of the axial compression apparatus. The experiment continues until the sample breaks. The sample is then removed from the apparatus. If the sample is intended for further study as a thin section, it is impregnated with epoxy and then cut to size at an angle normal to the fault plane.

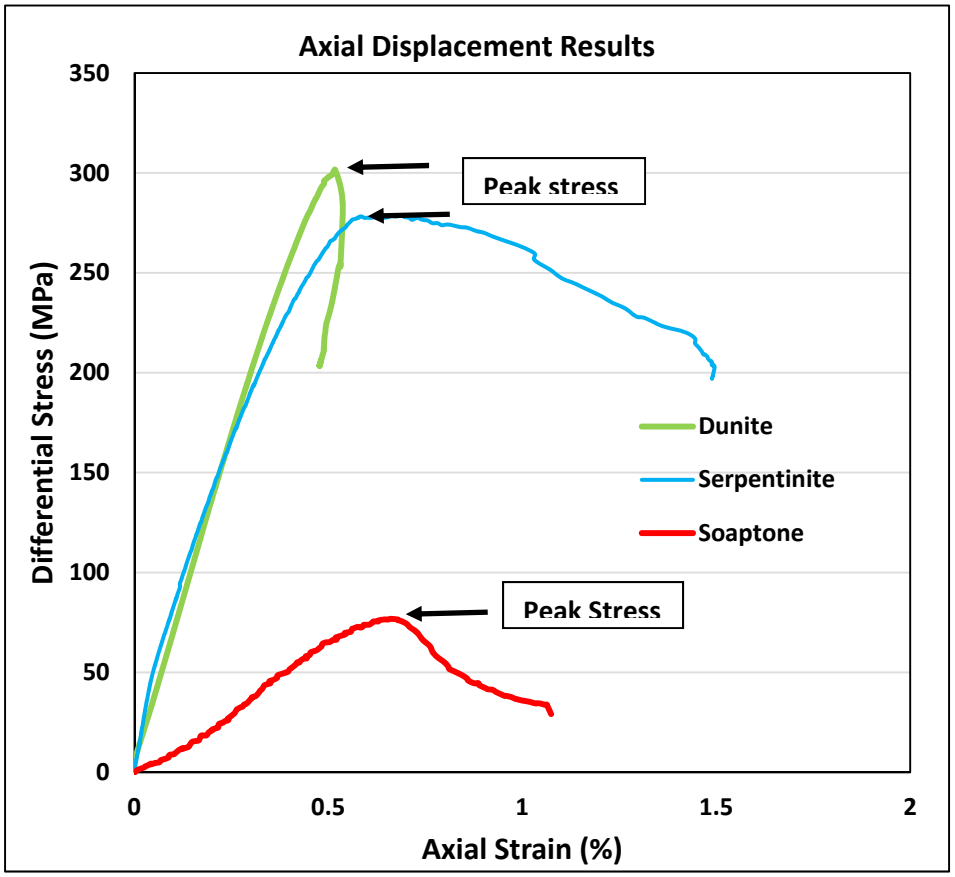

Figure 8. Graphed results from the deformation experiments. The arrows point to the peak stresses tolerated before sample failure.

We deformed dry samples to determine the maximum strength, strain, and mode of strain localization. The experiments were conducted at room temperature, confining pressure set to 50 MPa, and a constant strain rate of $3.5 \times 10^{-5}\ s^{-1}$. The differential stress, piston displacement, axial and radial strain of the sample was recorded during 2 second intervals of the experiment. The results were recorded at a high-gain frequency.

Due to time constraints only one deformation experiment was conducted for each rock type (figure 8). The stress-strain behavior was analyzed based on the model presented by

Patterson and Wong (2005), depicted in figure 9. The samples prepared for the listvenite experiment were not used due to large veins of quartz present. This heterogeneity in the samples could have affected the results. More adequate samples should be experimented on in the future, time did not allow for this to be done in my experiments.

VII. Deformation Results

a. Soapstone

During the beginning of the experiment with the soapstone sample, the response to loading reflects behavior associated with Stage I strain, which is referred to as the "settling-down" phase (Paterson and Wong, 2005). During this stage, the strain curve is concaved upward. This is associated with the closing of pre-existing cracks. Following the concaved portion of the curve is a straight, linear segment (Stage II). This is the elastic portion of the strain in the soapstone, at this point the deformation is still reversible. The peak stress tolerated by the soapstone before failure is 77 ± 1 MPa. This is recorded as the shear strength of this sample.

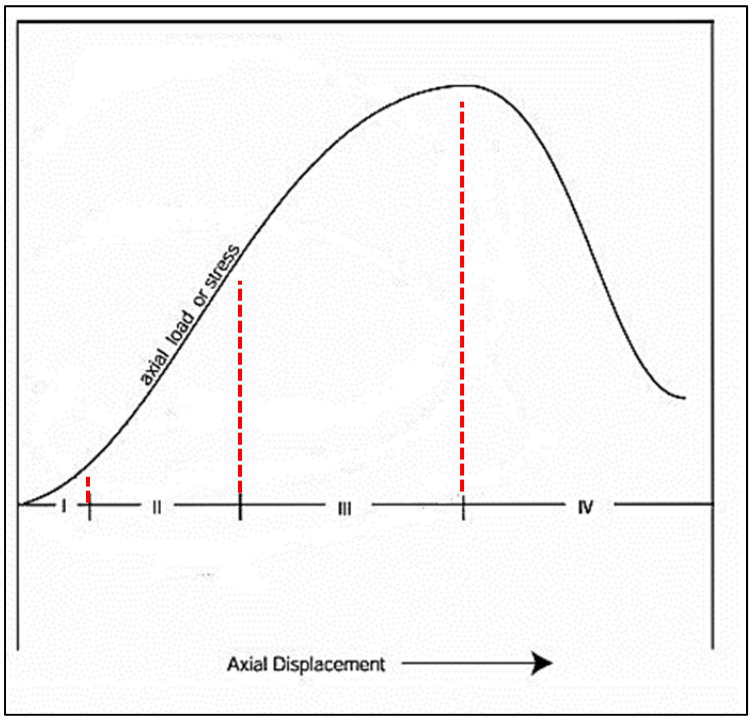

Figure 9: This image represents the four stages of strain during an axial loading experiment (highlighted by the dashed lines) as described by Patterson and Wong (2005).

b. Serpentinite

The serpentinite sample displays a slight curve in the strain at the beginning of the experiment. This can be associated with the settling and straightening experienced as the sample and piston as contact each other. There is a prominent elastic segment of the strain in the serpentinite, much larger than that of the soapstone. The peak stress is recorded as 279 ± 1 MPa. The post-failure behavior of the serpentinite exhibits a gradual reduction in loadbearing capability. Observations of the lithosphere (Kohlstedt et al., 1995) describe this as frictional sliding on existing fractures. This is described by Patterson and Wong (2005) as Stage IV, the onset of marked localization of microcrack development and the progression to macroscopic fracture.

c. Dunite

The dunite sample does not exhibit any curvature to its stress-strain behavior. The elastic portion of the strain curve is larger than that of the serpentinite. Stage III for this sample is very slight; it can be observed shortly before failure. Stage III is the departure from plastic behavior and the propagation of large numbers of microcracks. The peak stress recorded for the dunite

sample is 301 ± 1 MPa. There is a sudden drop in load bearing capability post-failure. This is described as cataclastic flow, which is dominated by brittle processes. Cataclasis is the pervasive brittle fracturing of rocks which is usually associated with faults and fault zones (Davis et al., 2012).

VIII. Discussion

The recorded porosity for the samples can be found in table 1 of the appendix. There was not a significant amount of variability between the different samples. Also found in table 1 is the elastic properties such as Young's moduli, Poisson's ratios, and the shear moduli. The data the electric resistivity experiments are not presented as a main focus due to the presence of magnesite, which could potentially have an effect on the recorded resistivity. They will be considered as more background can be developed. The results can be found in the appendix (graphs 1 & 2).

The results for the elastic wave velocities are also found in the appendix (table 2). The outcomes have been graphed along with previously results collected by H. Lisabeth using comparable samples (graph 3). The soapstone sample in my experiment yielded a much lower velocity then the soapstone tested in the experiment done by H. Lisabeth. There are several factors which can influence the wave speed measured in the experiments. Some of the factors that could have contributed to this variability are grain size and shape, anisotropy, and alteration zones within the sample (Khandelwal, 2013).

The samples from both sets of experiments (H. Lisabeth's and my own) came from the same locality. The densities of the samples from my experiment were similar for the serpentinite and soapstone. As mentioned before, the wave velocity, (V_p), is dependent on the density and elastic properties of the rock (Khandelwal, 2013). I statistically tested the results in order to decide if the samples could have come from the same population. The results from an unpaired student's t-test revealed that the difference was not considered to be statistically significantly.

During the deformation experiments, it was observed that there was a gradual reduction in shear strength from the dunite sample to the soapstone sample. As a response to the mineralization of olivine, the samples became less and less brittle due to their mineral composition. This inference is based on the transition of brittle failure as observed in dunite sample to the more ductile failure observed in both the serpentinite and soapstone samples. This could be due to the deformation behavior of the minerals present in the samples. It has been observed in experiments that phyllosilicates, talc and serpentine, will very easily slip as a result of weak bonding on the basal plane of the crystal structure (Escartin et al., 2008).

Corrections

There were some necessary corrections which needed to be done with the recorded results. The strain data were recorded at a high gain frequency, which has a shorter range but provides more accuracy. For this reason the recorded strain required a correction at each point where the displacement counter of the piston in the apparatus was "reset". There were artificial

gaps in the strain recorded which needed to be removed. These gaps were identified as artificial, based on the piston displacement measurements.

Additionally, the strain recorded for the soapstone sample needed to be calculated physically from the displacement, rather than taken from the recorded results. When analyzing the graphed results it was apparent that the sample deformed heterogeneously. This influenced the recorded strain during the experiment. Furthermore, the graphed results from the strain gauges indicated that the sample response was more rigid than typical for soapstone (graph 4). Therefore, to correct for the insufficient stain data, we needed to calculate the sample shortening using information recorded during the serpentinite experiment.

Displacement recorded during the experiment includes both machine and sample shortening. The serpentinite experiment had a similar set up to the soapstone experiment; from this data I was able to calculate the machine shortening during the experiment. This machine shortening was then subtracted from the displacement during the soapstone experiment. This data should sufficiently represent the axial strain recorded for the soapstone experiment. The plotted graphs are in the appendix (graphs 5 & 6). The radial strain recorded during the experiment was also affected but there was not an effective method available to calculate this data.

Error Analysis

Some of the natural variability in the experimental results can come from the fact that the samples tested came from an outcrop in the field rather than produced under controlled conditions. The samples will naturally have unique grain sizes and shapes, different quantities of minerals present, and have experienced different environmental conditions that can contribute to some variability in the experimental results. This heterogeneity can affect the overall shear strength of the samples. It is because of this reason that the samples intended for use in the listvenite experiment were omitted. The samples possessed large quartz veins when cut into right cylinders, which could result in localized strain during the experiment.

Due to limited time, we were only able to conduct one deformation experiment for each rock type. If we wanted to test the deformation results statistically, we would need to conduct at least two experiments with each rock to calculate a mean of the data. Therefore, without a comparison there could be variations, sample to sample, that are not apparent due to the limited data. In the future more experiment should be conducted to reinforce the outcomes from the experimental data collected during my project.

Implications

One of the most significant discussions about climate change is global warming and its drastic environmental consequences for mankind. The enhanced greenhouse effect associated to the combustion on fossil fuels has inspired the idea of long term carbon-dioxide (CO_2) storage by ex and in situ carbonation of minerals (Klein & Garrido, 2011). This process involves chemically bonding CO_2 within the crystal structure of minerals which contain divalent cations such as Mg^{2+}, Ca^{2+}, and Fe^{2+} (Klein & Garrido, 2011). The occurrences of low-temperature carbonated

ultramafic rocks found in nature suggest that conditions are favorable for CO_2 storage within shallow levels of the crust (Hansen et al., 2005).

Through studies of naturally produce carbonated peridotites, we can gain insight into the reaction mechanisms and the physicochemical feedback of the reaction process (Plumper et al., 2012). Currently, we have come up with an effective process for storage but the concern of CO_2 sequestration has not been resolved. As mentioned before, the change in shear strength due to olivine carbonation is unknown. Therefore, by quantifying the shear strength of the naturally carbonated ultramafic rocks, we will better understand the effects of CO_2 mineralization.

IX. Conclusion

From analysis of the data collected during the deformational experiments, there is a significant difference in the shear strength for the different rocks. There is a trend of reduction in shear strength as the rock becomes progressively altered. The change in mineral composition has been associated with this observation. This can be contributed to the presence of the minerals such as serpentine and talc. The presence of these two minerals has shown to have a considerable effect on the strength of the rocks found in the oceanic lithosphere (Escartin et al., 2001, 2008).

Experimental rock failure considered to be analogous to localized shear zones in the earth. Within these regions of the oceanic lithosphere, we observe sudden drops in load bearing capability. Activation of these shear zones produces slipping events such as earthquakes. Therefore, by recognizing the ubiquity of serpentine and talc within the lithosphere, we may be able to anticipate regions of potential weaknesses.

Due to the absence of experimental data for listvenite, we were not able to contribute the anticipated end member of peridotite carbonation. However the results from the experiments I conducted are in agreement with previous studies. Furthermore, it can be suggested from the preliminary results that there is a change which transpires in the rock's shear strength. As the oceanic lithosphere is progressively mineralized, the strength of the rocks is reduced.

References

Adelinet, M., Fortin, J. J., Schubnel, A. A., & Gueguen, Y. Y. (2013). Deformation modes in an Icelandic basalt; from brittle failure to localized deformation bands. Journal of Volcanology and Geothermal Research, 25515-25. doi:10.1016/j.jvolgeores.2013.01.011

Alexander, G., Maroto-Valer, M., & Gafarova-Aksoy, P. (2007). Evaluation of reaction variables in the dissolution of serpentine for mineral carbonation. Fuel [Guildford], 86(1-2), 273-281. doi:10.1016/j.fuel.2006.04.034

Asef, M., & Najibi, A. (2013). The effect of confining pressure on elastic wave velocities and dynamic to static Young's modulus ratio. Geophysics, 78(3), D135-d142. doi:10.1190/geo2012-0279.1

Bailey, E., & Holloway, J. R. (2000). Experimental determination of elastic properties of talc to 800 degrees C, 0.5 GPa; calculations of the effect on hydrated peridotite, and implications for cold subduction zones. Earth and Planetary Science Letters, 183(3-4), 487-498.

Beinlich, A., Plumper, O., Hovelmann, J., Austrheim, H., & Jamtveit, B. (2012). Massive serpentinite carbonation at Linnajavri, N-Norway. Terra Nova, 24(6), 446-455. doi:10.1111/j.1365-3121.2012.01083.x

Boschi, C., Früh-Green, G., & Escartín, J. (2006). OCCURRENCE AND SIGNIFICANCE OF SERPENTINITE-HOSTED, TALC- AND AMPHIBOLE-RICH FAULT ROCKS IN MODERN OCEANIC SETTINGS AND OPHIOLITE COMPLEXES: AN OVERVIEW. Ofioliti, 31(2), 129-140. doi:10.4454/ofioliti.v31i2.335

Burov, E. B. (2011). Rheology and strength of the lithosphere. Marine and Petroleum Geology, 28(8), 1402-1443. doi:10.1016/j.marpetgeo.2011.05.008

Candela, P.A. (1997). Chemical potential. Retreived from http://www.geol.umd.edu/facilities/lmdr/chmpot.htm

Davis, G.H., et al. (2012). Structural geology of rocks and regions (3rd ed). Hoboken, NJ: John Wiley & Sons, Inc.

Druiventak, A., Trepmann, C. A., Renner, J., & Hanke, K. (2011). Low-temperature plasticity of olivine during high stress deformation of peridotite at lithospheric conditions; an experimental study. Earth and Planetary Science Letters, 311(3-4), 199-211. doi:10.1016/j.epsl.2011.09.022

Escartin, J. J., Hirth, G. G., & Evans, B. B. (1997). Effects of serpentinization on the lithospheric strength and the style of normal faulting at slow-spreading ridges. Earth and Planetary Science Letters, 151(3-4), 181-189.

Escartin, J. J., Andreani, M. M., Hirth, G. G., & Evans, B. B. (2008). Relationships between the microstructural evolution and the rheology of talc at elevated pressures and temperatures. Earth and Planetary Science Letters, 268(3-4), 463-475. doi:10.1016/j.epsl.2008.02.004

Escartin, J. J., Hirth, G. G., & Evans, B. B. (2001). Strength of slightly serpentinized peridotites; implications for the tectonics of oceanic lithosphere. Geology [Boulder], 29(11), 1023-1026.

Grevemeyer, I., Ranero, C. R., Flueh, E. R., Klaeschen, D., & Bialas, J. (2007). Passive and active seismological study of bending-related faulting and mantle serpentinization at the Middle America Trench. Earth and Planetary Science Letters, 258(3-4), 528-542. doi:10.1016/j.epsl.2007.04.013

Hansen, L. D., Dipple, G. M., Gordon, T. M., & Kellett, D. A. (2005). Carbonated serpentinite (listwanite) at Atlin, British Columbia; a geological analogue to carbon dioxide sequestration. Canadian Mineralogist, 43, Part 1225-239.

Khandelwal, M. (2013). Correlating P-wave velocity with the physico-mechanical properties of different rocks. Pure And Applied Geophysics, 170(4), 507-514. doi:10.1007/s00024-012-0556-7

Klein, F., & Garrido, C. J. (2011). Thermodynamic constraints on mineral carbonation of serpentinized peridotite. Lithos [Oslo], 126(3-4), 147-160. doi:10.1016/j.lithos.2011.07.020

Kohlstedt, D. L., Evans, B., & Mackwell, S. J. (1995). Strength of the lithosphere; constraints imposed by laboratory experiments. Journal of Geophysical Research, 100(B9), 17. doi:10.1029/95JB01460

Lisabeth, H.P., Watter, K.E., & Zhu, W (2012). Effect of temperature on yielding behavior of carbonate rocks. American Rock Mechanics Association, 46th, 24-27.

Nilsson, L., & Lindahl, I. (2008). The talc/soapstone deposits in the Linnajavri area, Nordland, north Norwegian Caledonides. International Geological Congress, Abstracts = Congres Geologique International, Resumes, 33@Abstract1352652.

Olhoeft, G.R. (1985). Low-frequency electrical properties. Geophysics, Vol. 50. NO. 12, December 1985; 2492-2503.

Paterson, M.S., & Wong, T. (2005). Experimental rock deformation – The brittle field (2nd ed). The Netherlands: Springer.

Plumper, O., Piazolo, S., & Austrheim, H. (2012). Olivine pseudomorphs after serpentinized orthopyroxene record transient oceanic lithospheric mantle dehydration (Leka ophiolite complex, Norway). Journal of Petrology, 53(9), 1943-1968. doi:10.1093/petrology/egs039

Raleigh, C. B., & Paterson, M. S. (1965). Experimental deformation of serpentinite and its tectonic implications. Journal of Geophysical Research, 70(16), 3965-3985.

Regenauer-Lieb, K., & Yuen, D. A. (2006). Quartz rheology and short-time-scale crustal instabilities. Pure And Applied Geophysics, 163(9), 1915-1932. doi:10.1007/s00024-006-0104-4

Reynard, B. (2013). Serpentine in active subduction zones. Lithos [Oslo], 178171-185. doi:10.1016/j.lithos.2012.10.012

Rutter, E. H. (1986). On the nomenclature of mode of failure transitions in rocks. Tectonophysics, 122(3-4), 381-387.

Seeburger, D. A., & Nur, A. (1984). A pore space model for rock permeability and bulk modulus. Journal of Geophysical Research, 89(B1), 527-536. doi:10.1029/JB089iB01p00527

Shervais, J. W. (2001). Birth, death, and resurrection; the life cycle of suprasubduction zone ophiolites. *Geochemistry, Geophysics, Geosystems - G [Super 3]*, *2*(1), @paperno.2000GC000080.

Sousa, L. O. (2013). The influence of the characteristics of quartz and mineral deterioration on the strength of granitic dimensional stones. Environmental Earth Sciences, 69(4), 1333-1346. doi:10.1007/s12665-012-2036-x

Stixrude, L. (2002). Talc under tension and compression; spinodal instability, elasticity, and structure. Journal Of Geophysical Research, 107(B12), doi:10.1029/2001JB001684

Walsh, J. B. (1965). The effect of cracks in rocks on poisson's ratio. Journal of Geophysical Research, 70(20), 5249-5257.

Appendix:

Table 1.

Rock Type	Porosity (%)	Young's Modulus (GPa)	Poisson's Ratio	Shear Modulus (GPa)
Dunite	0.19 ± 0.23	-	-	-
Dunite	0.36 ± 0.23	-	-	-
Dunite	0.63 ± 0.23	64.2 ± 3.19	0.28 ± 0.01	25.2
Serpentinite	0.27	50.0 ± 12.3	0.44 ± 0.03	17.4
Soapstone	0.28	14.4 ± 1.26	-	-

Data recorded with σ_1

Table 2.

Rock Type	Vp (km/s)	Density (g/cm^3)
Serpentinite	6.267 ± 0.02	2.71
Soapstone	2.865 ± 2.44	2.77
Results from H.Lisabeth	**Vp (km/s)**	
Serpentinite	6.243 ± 0.02	
Soapstone	6.321 ± 2.44	

Data recorded with σ1

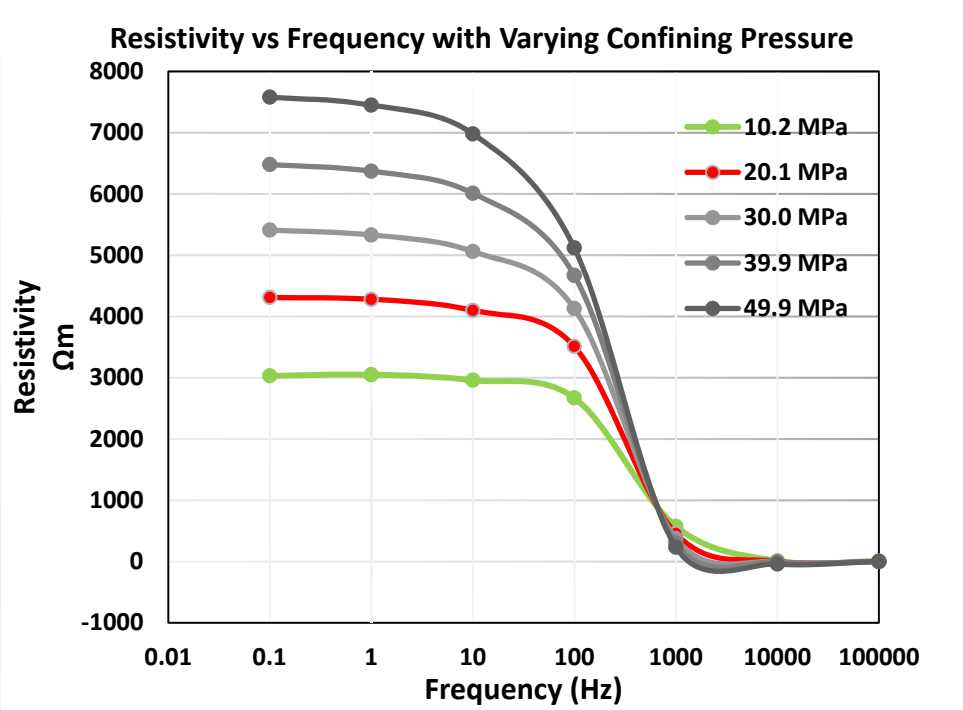

Graph 1. Electrical resistivity for serpentinite based on confining pressures. This graph is displaying the recorded resistivities in Ohm meters on the y-axis and the frequency settings during the experiment. Each curve is plotted for the different confining pressures set.

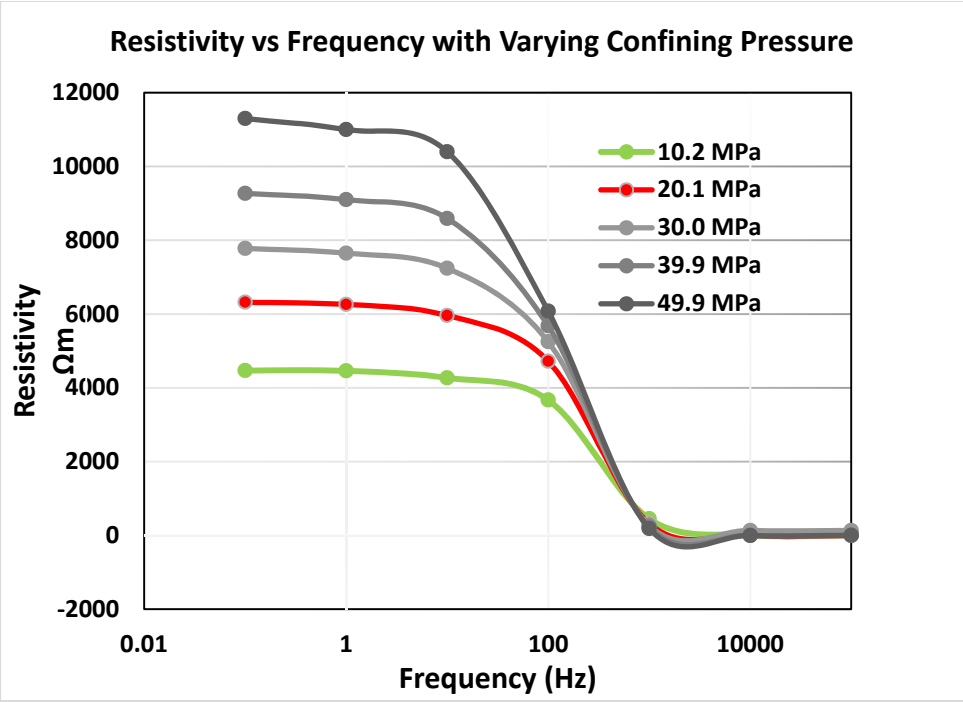

Graph 2. Electrical resistivity for soapstone based on confining pressures. This graph is displaying the recorded resistivities in Ohm meters on the y-axis and the frequency settings during the experiment. Each curve is plotted for the different confining pressures set.

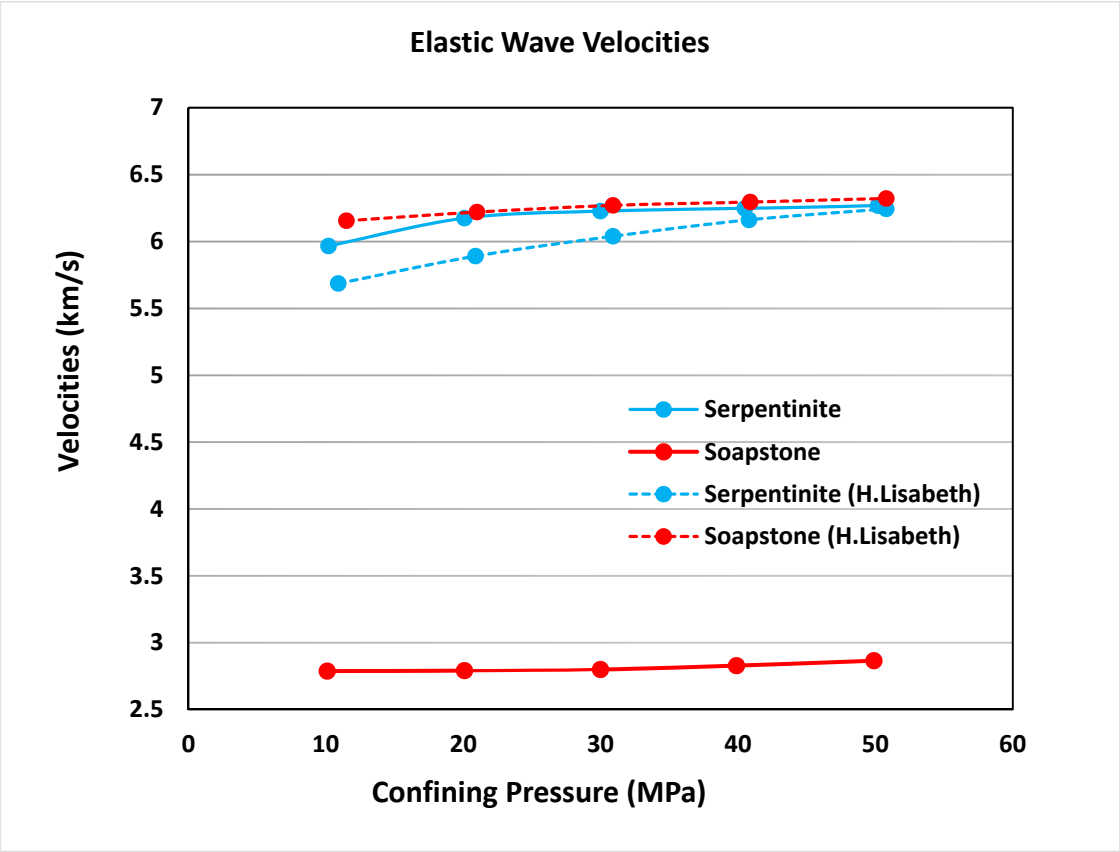

Graph 3. Elastic wave velocities recorded for samples of soapstone and serpentinite. The y-axis displays the velocities of the wave speeds in kilometers per second. On the x-axis can be found the confining pressure during the recording of the wave speeds. This graph displays my experimental results paralleled to results from experiments conducted by H. Lisabeth.

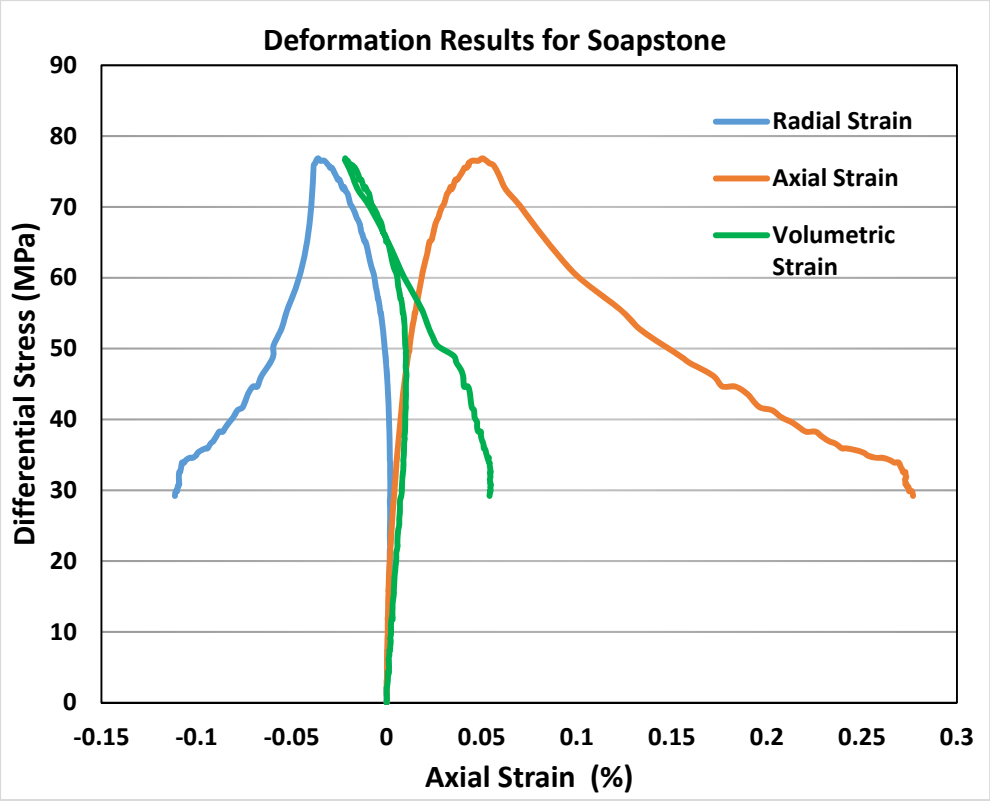

Graph 4. This graph displays the recorded results from the experiment conducted with the soapstone sample. The differential stress in recorded on the y-axis and the x-axis displays the axial strain. Based on referencing past studies of minerals (e.g. talc), the strain recorded should have been larger due to yielding behavior of the minerals present (Escartin et al., 2008).

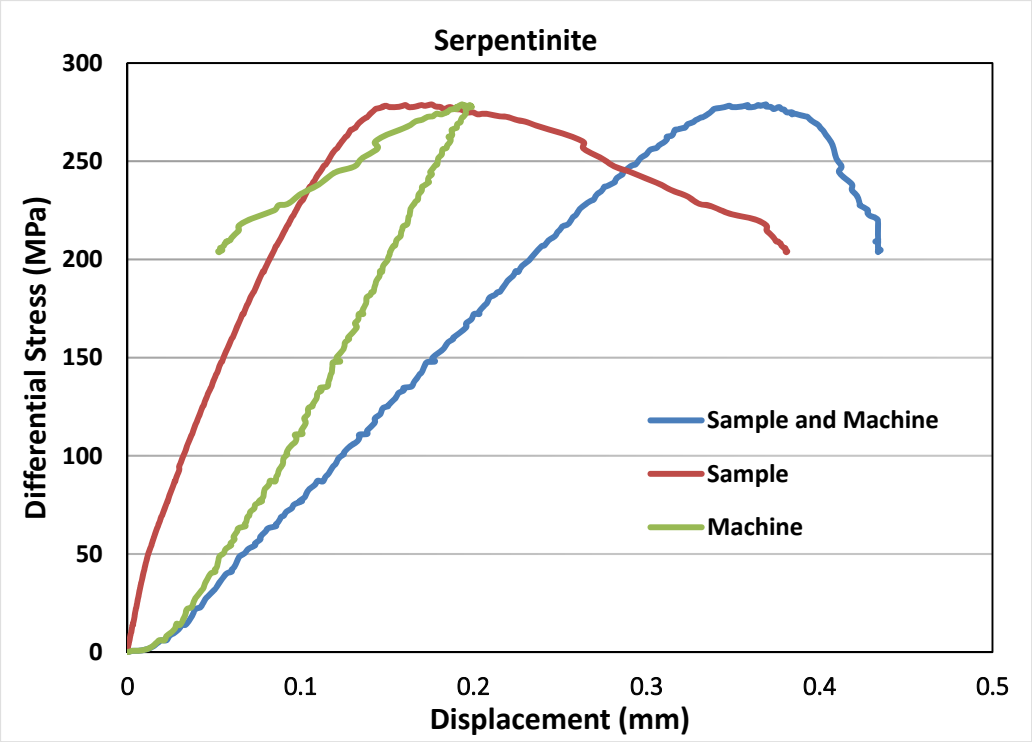

Graph 5. This graph displays the different displacements recorded in the serpentinite experiment. The differential stress is found on the y-axis and the displacement is on the x-axis. The data collected from the soapstone experiment was not used due to heterogeneous failure, which resulted with erroneous data. Therefore, we used the serpentinite data collected of axial strain and piston displacement (which includes the sample and the piston of the apparatus). From this data I calculated the machine shortening for this experiment. The machine shortening from this experiment was the used to calculating the soapstone shortening.

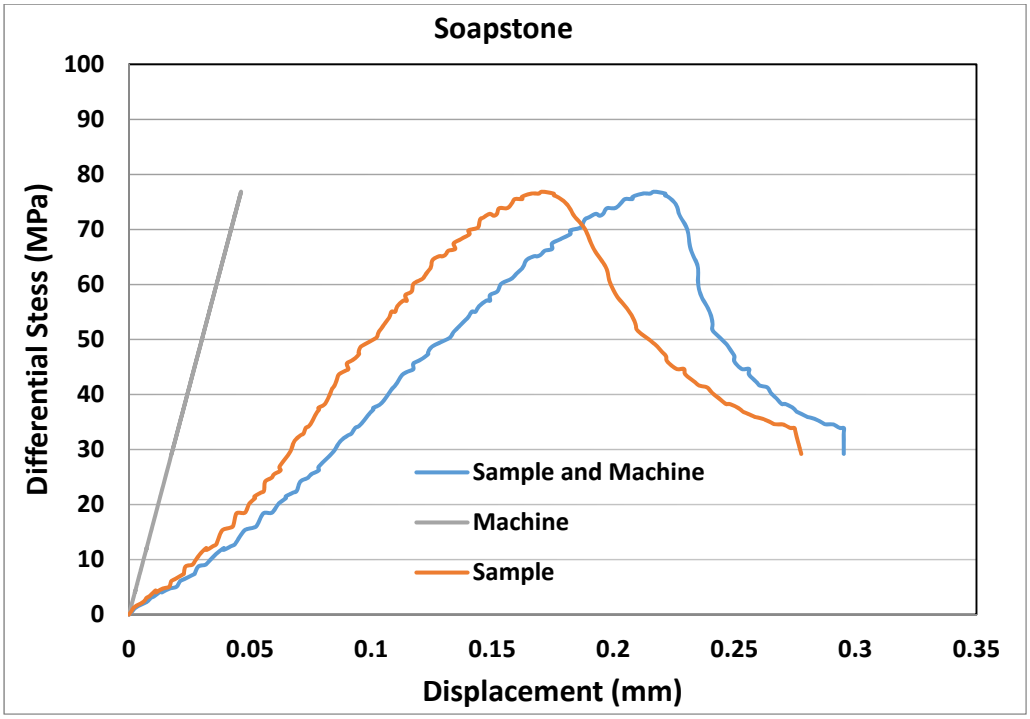

Graph 6. The graph shows the calculated axial displacement for the soapstone sample. The y-axis displays the differential stress and the x-axis displays the displacement. The machine displacement was recorded from the serpentinite experiment. This value was then subtracted from the combined machine and sample displacement.

Data Table 1.

Dunite Axial Strain	Dunite Radial Strain	Differential Stress	Serpentinite Axial Strain	Serpentinite Radial Strain	Differential Stress	Soapstone Axial Strain	Differential Stress
%	%	MPa	%	%	MPa	%	MPa
0.000	0.000	0.000	0.000	0.000	0.000	0.000	0.000
0.000	0.000	0.160	0.000	0.000	0.336	0.004	0.671
-0.001	0.000	0.479	0.000	0.000	0.671	0.009	1.342
-0.001	0.000	0.798	0.000	0.000	0.671	0.019	2.014
-0.002	0.000	1.117	0.000	0.000	1.007	0.024	2.349
-0.002	0.000	1.436	0.000	0.000	1.007	0.028	3.020
-0.003	-0.001	1.755	0.000	0.000	1.342	0.033	3.356
-0.003	-0.001	1.915	0.001	0.000	1.678	0.042	4.363
-0.003	-0.001	2.074	0.002	-0.001	3.020	0.043	4.027
-0.003	-0.001	2.234	0.003	-0.001	4.027	0.053	4.698
-0.004	-0.001	2.553	0.004	-0.001	5.034	0.064	5.034
-0.003	-0.001	2.713	0.004	-0.002	6.041	0.068	6.041

-0.003	-0.001	3.351	0.005	-0.002	6.041	0.073	6.376
-0.003	-0.001	3.830	0.006	-0.002	8.054	0.078	6.712
-0.002	-0.001	4.468	0.007	-0.003	9.061	0.088	7.383
-0.001	-0.001	5.106	0.008	-0.003	9.732	0.088	7.383
0.000	-0.002	5.745	0.010	-0.003	12.081	0.090	8.725
0.001	-0.002	6.542	0.013	-0.004	14.430	0.101	9.061
0.002	-0.002	7.181	0.012	-0.004	13.759	0.106	9.732
0.003	-0.002	7.659	0.013	-0.004	14.766	0.110	10.403
0.004	-0.003	8.617	0.015	-0.005	16.780	0.114	11.075
0.005	-0.003	8.936	0.017	-0.005	18.793	0.123	12.081
0.006	-0.003	9.893	0.019	-0.006	21.813	0.124	11.746
0.007	-0.003	10.532	0.020	-0.007	22.820	0.134	12.417
0.009	-0.004	11.489	0.022	-0.007	24.834	0.139	12.753
0.010	-0.004	12.287	0.024	-0.008	27.183	0.143	13.759
0.011	-0.004	13.244	0.025	-0.008	28.525	0.146	14.766
0.013	-0.005	14.361	0.027	-0.009	31.210	0.150	15.437
0.014	-0.005	14.840	0.029	-0.009	32.552	0.161	15.773
0.016	-0.005	15.957	0.031	-0.010	34.902	0.166	16.108
0.018	-0.006	17.074	0.033	-0.011	36.579	0.169	17.451
0.019	-0.006	18.031	0.036	-0.012	39.935	0.173	18.458
0.021	-0.007	18.829	0.037	-0.012	40.942	0.184	18.458
0.022	-0.007	19.787	0.038	-0.013	41.949	0.189	19.129
0.024	-0.008	21.063	0.039	-0.013	43.291	0.192	20.136
0.026	-0.008	22.180	0.042	-0.014	45.976	0.201	21.142
0.028	-0.009	23.616	0.045	-0.015	48.661	0.201	21.478
0.030	-0.009	24.414	0.048	-0.016	50.339	0.211	22.149
0.032	-0.010	25.691	0.050	-0.017	52.017	0.216	22.485
0.034	-0.010	27.127	0.052	-0.017	53.023	0.218	24.163
0.036	-0.011	28.244	0.054	-0.018	54.366	0.228	24.834
0.038	-0.011	29.361	0.055	-0.019	55.373	0.232	25.505
0.040	-0.012	30.797	0.058	-0.020	57.386	0.242	26.176
0.043	-0.013	32.393	0.060	-0.020	58.728	0.240	26.847
0.045	-0.013	33.988	0.064	-0.022	61.413	0.249	28.190
0.048	-0.014	35.903	0.067	-0.023	63.091	0.253	28.861
0.051	-0.015	37.658	0.069	-0.023	64.098	0.257	29.532
0.053	-0.016	39.095	0.070	-0.024	65.105	0.261	30.539
0.056	-0.016	41.009	0.073	-0.025	66.447	0.264	31.546
0.058	-0.017	42.445	0.076	-0.026	68.796	0.274	32.552
0.060	-0.018	43.882	0.078	-0.026	69.467	0.279	32.888
0.063	-0.018	45.477	0.081	-0.028	71.481	0.282	33.895
0.066	-0.019	47.711	0.084	-0.029	73.159	0.287	34.230

0.069	-0.020	49.626	0.088	-0.030	75.172	0.292	34.902
0.072	-0.021	51.541	0.091	-0.031	76.851	0.299	36.579
0.075	-0.022	53.456	0.091	-0.031	76.851	0.304	37.251
0.077	-0.022	55.051	0.094	-0.032	78.864	0.303	37.586
0.080	-0.024	57.285	0.098	-0.033	81.549	0.313	38.257
0.083	-0.024	58.881	0.101	-0.035	83.227	0.321	39.935
0.086	-0.025	60.955	0.104	-0.036	85.240	0.324	40.942
0.089	-0.026	62.711	0.107	-0.037	87.254	0.328	41.613
0.091	-0.027	64.466	0.108	-0.037	86.918	0.332	42.620
0.095	-0.028	66.700	0.111	-0.038	89.267	0.335	43.627
0.097	-0.028	68.455	0.114	-0.039	90.610	0.345	44.298
0.101	-0.029	70.689	0.117	-0.041	92.623	0.351	44.634
0.103	-0.030	72.604	0.117	-0.042	94.637	0.348	45.640
0.107	-0.031	74.998	0.120	-0.043	95.979	0.358	46.312
0.110	-0.032	77.072	0.124	-0.044	98.664	0.368	47.318
0.113	-0.033	78.827	0.128	-0.045	100.678	0.367	47.654
0.115	-0.033	80.263	0.129	-0.046	101.349	0.370	48.661
0.118	-0.034	82.178	0.132	-0.047	103.027	0.380	49.332
0.122	-0.035	84.571	0.136	-0.048	105.376	0.385	49.668
0.125	-0.036	86.646	0.139	-0.050	107.054	0.395	50.339
0.127	-0.037	88.401	0.142	-0.051	109.067	0.399	51.345
0.130	-0.038	90.156	0.145	-0.052	110.745	0.403	52.017
0.133	-0.039	92.550	0.147	-0.053	111.081	0.412	53.359
0.136	-0.039	94.465	0.149	-0.054	112.759	0.416	54.030
0.140	-0.040	96.698	0.153	-0.055	115.444	0.419	55.037
0.142	-0.041	98.294	0.157	-0.056	117.121	0.425	55.037
0.145	-0.042	100.209	0.160	-0.058	119.135	0.429	56.044
0.148	-0.043	102.283	0.164	-0.059	121.149	0.438	57.051
0.151	-0.044	104.517	0.168	-0.061	124.169	0.444	57.051
0.155	-0.045	106.751	0.171	-0.062	125.176	0.442	58.057
0.158	-0.045	108.826	0.172	-0.063	125.511	0.452	58.728
0.160	-0.046	110.741	0.176	-0.064	128.196	0.454	60.071
0.164	-0.047	112.815	0.179	-0.065	129.538	0.464	60.742
0.167	-0.048	115.049	0.183	-0.067	131.887	0.470	61.078
0.169	-0.049	116.325	0.186	-0.068	133.230	0.474	61.749
0.171	-0.049	118.081	0.188	-0.069	134.572	0.478	62.420
0.175	-0.050	120.474	0.190	-0.070	135.243	0.482	63.091
0.178	-0.051	122.868	0.194	-0.071	137.593	0.485	64.434
0.182	-0.052	125.102	0.197	-0.072	139.270	0.495	65.105
0.185	-0.053	127.336	0.200	-0.074	141.284	0.501	65.105
0.188	-0.054	129.091	0.204	-0.075	142.626	0.506	65.440

0.191	-0.055	131.325	0.208	-0.077	145.647	0.510	66.111
0.195	-0.056	133.719	0.212	-0.079	147.660	0.521	66.447
0.198	-0.057	135.474	0.214	-0.080	147.996	0.519	67.454
0.200	-0.057	137.069	0.217	-0.081	149.674	0.529	68.125
0.203	-0.058	139.144	0.221	-0.082	152.023	0.534	68.461
0.206	-0.059	141.218	0.225	-0.084	154.036	0.544	69.132
0.210	-0.060	143.293	0.228	-0.086	155.714	0.542	69.803
0.213	-0.061	145.686	0.232	-0.087	157.728	0.553	70.139
0.216	-0.062	147.441	0.235	-0.088	159.406	0.558	70.474
0.219	-0.063	149.356	0.238	-0.090	160.077	0.561	71.816
0.223	-0.064	151.909	0.240	-0.090	161.084	0.566	72.152
0.226	-0.065	154.143	0.243	-0.092	163.097	0.576	72.823
0.229	-0.065	155.420	0.247	-0.093	165.447	0.583	72.488
0.231	-0.066	157.335	0.251	-0.095	167.460	0.588	72.823
0.235	-0.067	159.569	0.256	-0.097	169.474	0.591	73.830
0.238	-0.068	161.962	0.260	-0.099	172.158	0.603	73.830
0.241	-0.069	163.877	0.262	-0.100	172.158	0.608	74.166
0.245	-0.070	166.271	0.265	-0.101	173.501	0.612	74.837
0.247	-0.070	167.547	0.270	-0.103	176.521	0.617	75.508
0.251	-0.071	169.622	0.273	-0.105	177.863	0.628	75.508
0.254	-0.072	172.015	0.278	-0.107	180.548	0.627	75.844
0.258	-0.073	174.568	0.281	-0.108	181.891	0.632	76.179
0.260	-0.074	175.526	0.285	-0.110	183.233	0.643	76.515
0.263	-0.075	177.600	0.286	-0.111	183.569	0.649	76.515
0.267	-0.076	179.994	0.290	-0.112	185.582	0.655	76.515
0.270	-0.077	181.908	0.294	-0.114	187.260	0.660	76.850
0.273	-0.077	184.302	0.297	-0.115	189.274	0.678	76.515
0.276	-0.078	185.898	0.302	-0.117	191.623	0.679	76.179
0.279	-0.079	187.812	0.307	-0.120	193.972	0.686	75.844
0.283	-0.080	190.046	0.308	-0.120	193.636	0.700	74.501
0.286	-0.081	191.961	0.312	-0.122	195.985	0.711	72.488
0.288	-0.081	192.919	0.316	-0.124	197.328	0.728	70.139
0.291	-0.082	194.674	0.320	-0.125	199.341	0.743	66.447
0.294	-0.083	196.589	0.324	-0.127	201.019	0.762	63.091
0.298	-0.084	198.982	0.327	-0.129	202.362	0.768	60.406
0.302	-0.085	201.376	0.331	-0.131	204.040	0.780	57.722
0.305	-0.086	203.450	0.336	-0.133	206.724	0.797	55.373
0.308	-0.087	205.525	0.338	-0.134	207.060	0.809	53.023
0.312	-0.088	207.439	0.342	-0.136	208.738	0.812	51.681
0.315	-0.089	209.673	0.345	-0.138	210.080	0.827	50.339
0.318	-0.089	211.269	0.349	-0.140	211.758	0.841	48.996

0.320	-0.090	212.386	0.353	-0.142	213.772	0.850	47.990
0.323	-0.091	214.301	0.357	-0.144	215.114	0.858	46.983
0.327	-0.092	216.535	0.361	-0.146	216.792	0.860	45.976
0.331	-0.093	218.769	0.364	-0.147	217.799	0.875	44.634
0.335	-0.094	221.003	0.367	-0.149	219.477	0.887	44.634
0.338	-0.095	222.918	0.372	-0.151	221.490	0.889	43.627
0.341	-0.095	224.673	0.375	-0.153	222.497	0.904	42.285
0.344	-0.096	226.588	0.380	-0.156	224.511	0.911	41.613
0.348	-0.097	228.343	0.384	-0.158	226.189	0.924	41.278
0.350	-0.097	229.460	0.389	-0.161	228.202	0.932	40.271
0.353	-0.098	231.375	0.392	-0.163	229.209	0.939	39.600
0.357	-0.099	233.449	0.395	-0.164	229.880	0.947	38.929
0.361	-0.100	235.524	0.398	-0.166	230.551	0.954	38.257
0.364	-0.101	237.438	0.402	-0.168	232.900	0.960	38.257
0.367	-0.102	239.194	0.407	-0.171	234.914	0.973	37.586
0.371	-0.103	241.108	0.412	-0.174	236.927	0.980	36.915
0.375	-0.103	243.023	0.416	-0.176	237.263	0.987	36.579
0.378	-0.104	245.098	0.420	-0.179	239.277	1.000	35.908
0.381	-0.105	246.374	0.422	-0.181	239.612	1.000	35.908
0.383	-0.105	247.651	0.427	-0.183	241.626	1.013	35.573
0.387	-0.106	250.044	0.431	-0.186	243.304	1.019	35.237
0.391	-0.107	251.959	0.435	-0.188	244.311	1.026	34.902
0.395	-0.108	254.193	0.438	-0.191	245.317	1.032	34.566
0.398	-0.109	255.470	0.443	-0.193	247.331	1.044	34.566
0.402	-0.110	257.225	0.447	-0.196	248.002	1.051	34.230
0.406	-0.110	259.459	0.449	-0.197	248.338	1.057	33.895
0.409	-0.111	261.055	0.453	-0.200	250.016	1.063	33.895
0.413	-0.112	262.650	0.458	-0.203	251.694	1.065	33.224
0.415	-0.113	264.086	0.462	-0.206	253.371	1.065	32.888
0.419	-0.114	266.001	0.467	-0.210	255.049	1.066	32.552
0.422	-0.114	267.597	0.471	-0.213	256.056	1.066	32.552
0.426	-0.115	269.193	0.475	-0.215	256.727	1.067	32.217
0.430	-0.116	271.267	0.479	-0.218	258.070	1.068	31.881
0.433	-0.117	272.863	0.484	-0.222	259.748	1.069	31.546
0.437	-0.117	274.618	0.489	-0.225	261.090	1.069	31.210
0.441	-0.118	276.852	0.494	-0.229	262.432	1.070	30.874
0.446	-0.119	278.767	0.498	-0.232	263.104	1.070	30.874
0.450	-0.120	279.884	0.505	-0.237	265.788	1.071	30.539
0.453	-0.120	281.001	0.509	-0.241	266.124	1.071	30.539
0.456	-0.121	282.596	0.513	-0.244	266.795	1.072	30.203
0.460	-0.121	284.511	0.516	-0.247	267.131	1.072	29.868

0.465	-0.122	286.266	0.521	-0.250	268.809	1.072	29.868
0.468	-0.122	287.224	0.526	-0.254	269.815	1.072	29.868
0.472	-0.123	288.660	0.531	-0.258	270.822	1.073	29.532
0.476	-0.124	290.575	0.535	-0.262	271.493	1.074	29.196
0.482	-0.124	292.809	0.540	-0.265	272.165		
0.486	-0.125	293.766	0.543	-0.268	272.500		
0.489	-0.125	294.724	0.549	-0.273	274.178		
0.489	-0.125	296.000	0.555	-0.278	275.185		
0.495	-0.126	297.117	0.561	-0.283	276.527		
0.501	-0.126	298.234	0.567	-0.289	276.863		
0.507	-0.126	298.713	0.572	-0.295	277.198		
0.512	-0.126	299.830	0.578	-0.301	277.534		
0.518	-0.127	301.426	0.578	-0.306	277.870		
0.536	-0.128	285.628	0.585	-0.313	278.205		
0.531	-0.124	253.076	0.593	-0.313	277.534		
0.531	-0.124	254.353	0.601	-0.320	277.534		
0.530	-0.124	254.353	0.609	-0.326	277.534		
0.528	-0.124	253.714	0.619	-0.333	277.870		
0.526	-0.123	252.597	0.629	-0.339	278.541		
0.525	-0.123	251.480	0.636	-0.344	277.534		
0.523	-0.122	249.725	0.644	-0.349	277.534		
0.521	-0.120	246.853	0.654	-0.354	277.870		
0.508	-0.112	234.247	0.664	-0.359	278.541		
0.496	-0.106	225.471	0.674	-0.365	278.205		
0.494	-0.105	223.875	0.687	-0.372	278.876		
0.493	-0.104	222.439	0.696	-0.376	277.870		
0.492	-0.102	220.684	0.708	-0.381	277.534		
0.491	-0.100	218.769	0.716	-0.384	276.527		
0.490	-0.099	217.652	0.729	-0.389	277.534		
0.490	-0.098	216.854	0.741	-0.394	276.527		
0.489	-0.097	216.216	0.755	-0.398	276.192		
0.489	-0.096	215.418	0.768	-0.402	274.849		
0.489	-0.095	214.460	0.781	-0.406	274.849		
0.489	-0.095	213.982	0.792	-0.409	273.843		
0.488	-0.094	212.865	0.809	-0.414	274.178		
0.488	-0.093	211.907	0.826	-0.419	273.507		
0.489	-0.093	212.226	0.842	-0.423	272.836		
0.488	-0.092	210.950	0.860	-0.428	272.500		
0.486	-0.091	209.514	0.877	-0.432	271.158		
0.485	-0.091	208.716	0.899	-0.437	270.151		
0.484	-0.091	208.078	0.921	-0.441	268.473		

0.483	-0.090	207.439	0.942	-0.445	266.795
0.483	-0.090	207.280	0.963	-0.448	265.453
0.482	-0.090	206.801	0.993	-0.452	263.439
0.481	-0.090	206.482	1.031	-0.455	259.748
0.481	-0.089	206.322	1.031	-0.460	256.392
0.481	-0.090	206.322	1.073	-0.464	251.358
0.481	-0.089	206.163	1.101	-0.468	247.331
0.481	-0.089	206.003	1.135	-0.473	244.646
0.480	-0.089	205.684	1.168	-0.477	241.626
0.480	-0.089	205.365	1.204	-0.482	238.270
0.479	-0.089	205.046	1.230	-0.483	235.250
0.479	-0.089	204.886	1.265	-0.484	232.229
0.479	-0.089	205.046	1.293	-0.483	228.202
0.479	-0.089	205.046	1.314	-0.483	227.531
0.479	-0.089	204.727	1.340	-0.484	225.182
0.479	-0.088	204.567	1.359	-0.484	223.504
0.479	-0.088	204.567	1.381	-0.484	222.161
0.478	-0.088	204.088	1.404	-0.485	221.155
0.478	-0.088	203.929	1.426	-0.485	219.812
0.478	-0.088	203.929	1.445	-0.485	217.128
0.478	-0.088	203.769	1.445	-0.484	214.778
0.477	-0.088	203.450	1.453	-0.483	213.101
0.477	-0.088	203.610	1.458	-0.483	211.758
0.477	-0.088	203.450	1.462	-0.482	210.751
0.477	-0.088	203.610	1.465	-0.482	209.745
0.477	-0.088	203.769	1.468	-0.482	209.073
0.477	-0.088	203.610	1.471	-0.482	209.073
0.477	-0.088	203.769	1.474	-0.481	208.402
0.477	-0.088	203.450	1.477	-0.481	208.067
			1.479	-0.481	207.060
			1.480	-0.481	206.724
			1.482	-0.480	206.389
			1.484	-0.480	206.053
			1.486	-0.480	205.718
			1.488	-0.480	205.718
			1.489	-0.480	204.711
			1.488	-0.479	204.040
			1.489	-0.479	203.704
			1.491	-0.479	203.704
			1.492	-0.479	204.040

"I pledge on my honor that I have not given or received any unauthorized assistance on this assignment."

Thomas Braga